Cell Stress and Chaperones (2025) 30:xxx–xxx
https://doi.org/10.1016/j.cstres.2025.100084

Heat shock induces alternative polyadenylation through dynamic DNA methylation and chromatin looping

Emily E. Fink[1,†] · **Yi Zhang**[2,3,†] · **Briana Santo**[2] · **Anwita Siddavatam**[2] · **Rosie Ou**[2] · **Vishal Nanavaty**[1,4,5,6] · **Byron H. Lee**[7] · **Angela H. Ting**[1,2,*]

Received: 30 April 2025 / Revised: 18 May 2025 / Accepted: 21 May 2025

Abstract

Alternative cleavage and polyadenylation (APA) is a gene regulatory mechanism used by cells under stress to up-regulate proteostasis-promoting transcripts, but how cells achieve this remains poorly understood. Previously, we elucidated a DNA methylation-regulated APA mechanism, in which gene body DNA methylation enhances distal poly(A) isoform expression by blocking CCCTC-binding factor (CTCF) binding and chromatin loop formation at APA control regions. We hypothesized that DNA methylation-regulated APA is one mechanism cells employ to induce proteostasis-promoting poly(A) isoforms. At the *DNAJB6* cochaperone locus, acute heat shock resulted in binding of stress response transcription factors heat shock factor 1, ATF6, and YY1 at the APA control region and an increase in the expression of the proximal poly(A) isoform known to prevent protein aggregation. Furthermore, TET1 was recruited to rapidly demethylate DNA, facilitating CTCF binding and chromatin loop formation, thereby reinforcing preferential proximal poly(A) isoform expression. As cells recovered, the transcription factors vacated the APA control region, and DNMT1 was recruited to remethylate the region. This process resolved chromatin looping and reset the poly(A) isoform expression pattern. Our findings unveil an epigenetic mechanism enabling cells to dynamically modulate poly(A) isoforms in response to stress while shedding light on the interplay between DNA methylation, transcription factor binding, and chromatin looping.

Keywords Heat shock · DNA methylation · Chromatin · DNAJB6 · Alternative polyadenylation

Abbreviations: APA,, alternative cleavage and polyadenylation; CTCF, CCCTC-binding factor; poly(A), polyadenylation; HSR, heat-shock response; UPR, unfolded protein response; ER, endoplasmic reticulum; HS, heat shock; 3' UTR, 3' untranslated region; GO, gene ontology

† These authors contributed equally to this work.

* Angela H. Ting
ahting@mdanderson.org

1 Genomic Medicine, Lerner Research Institute, Cleveland Clinic, Cleveland, OH 44195, USA

2 Department of Epigenetics and Molecular Carcinogenesis, University of Texas MD Anderson Cancer Center, Houston, TX 77030, USA

3 Department Gastrointestinal Surgery, Affiliated Hospital of Xuzhou Medical University, Xuzhou, Jiangsu, China

4 Department of Life Science, Food and Nutrition Science, Gujarat University, Ahmedabad, Gujarat, India

5 Neuberg Center for Genomic Medicine, Neuberg Supratec Reference Laboratory, Ahmedabad, Gujarat, India

6 Department of Biological Sciences, Sandip Bhavini Research Institute, Ahmedabad, Gujarat, India

7 Department of Urology, University of Texas MD Anderson Cancer Center, Houston, TX 77030, USA.

Published online: 22 May 2025

Introduction

The cellular response to perturbations in proteostasis includes the compartment-specific heat-shock response (HSR) in the cytosol and the unfolded protein response (UPR) in the endoplasmic reticulum (ER), with significant crosstalk between both pathways.[1] The HSR and UPR are multifaceted and evolutionarily conserved signaling pathways aimed at inducing an anti-stress proteome. If the cell is unable to resolve the stress, apoptosis ensues.[2] In eukaryotic organisms, the cascade of signals involved in the cell stress response has been significantly studied at the transcriptional, translational, and post-translational levels. The canonical events involved in the HSR include the induction of the transcription factor heat shock factor 1 (HSF1), which promotes the transcription of heat shock (HS) proteins.[3] The key events involved in the UPR include the post-translational activation of ER-membrane associated proteins, IRE-1, PERK, and ATF6, upon presence of misfolded proteins in the ER lumen, followed by translational attenuation, regulated IRE-1-dependent decay of messenger RNA, and selective transcriptional upregulation of proteostasis-promoting genes *via* transcription factors XBP-1s, ATF4, and ATF6.[1,2,4,5,6] Furthermore, recent efforts have highlighted additional layers of regulation during the cell stress response at the level of post-transcriptional messenger RNA processing, specifically alternative cleavage and polyadenylation (APA).[5,7]

About 70–80% of human genes can be terminated at multiple polyadenylation [poly(A)] sites, giving rise to distinct messenger RNA (mRNA) isoforms with contrasting properties. These alternative poly(A) isoforms can differ in their 3′ untranslated region (UTR) lengths or in amino acid coding content. Differences in 3′ UTR lengths can affect mRNA metabolism and ultimately the expression of the final protein. For example, longer 3′ UTRs can harbor binding sites for RNA binding protein or micro-RNA, which can modulate mRNA half-life, alter mRNA localization, or modify translation efficiency.[5] Alternative intronic poly(A) sites can generate distinct protein isoforms, many of which have unique functions. Thus, it is not surprising that the cellular response to proteotoxic stress can utilize APA as a mechanism to selectively express proteostasis-promoting transcripts while simultaneously suppressing overall transcription and translation. For instance, 3′ UTR global shortening has been observed in cells exposed to arsenic stress as an adaptive mechanism to preserve mRNAs during recovery from stress.[5] Global APA changes have also been observed following stressors such as HS,[8] nutrient deficiency,[9] DNA damage,[10] and oxidative stress.[5,11] While the underlying mechanism dictating poly(A) site usage is largely unknown, it has been suggested that epigenetic features and chromatin structure can be altered during stress and recovery[12] and should be explored as a potential mechanism.

DNA methylation changes have been observed during environmental HS of organisms within the livestock industry.[13,14] Pathophysiological hypermethylation of ER stress genes has been observed in association with insulin resistance[15,16] and cancer.[17] DNA demethylation has also been observed during the cellular response to ER stress in lens epithelial cells.[18] While stress-induced alterations in DNA methylation patterns have been documented, their impact on the transcriptome is not well understood. We previously described a mechanism by which DNA methylation regulates APA through CCCTC-binding factor (CTCF)/cohesin-mediated chromatin looping.[19] We identified 546 genes undergoing APA between a pair of isogenic colon cancer cell lines that differ in their genomic DNA methylation levels. A subset of these genes has differential DNA methylation between their alternative poly(A) sites. In the absence of DNA methylation, CTCF binds its recognition motif in these regions to facilitate cohesin complex docking and chromatin loop contact formation. Coincident with the loop contact point, we also observed recruitment of serine 5 phosphorylated RNA polymerase II (Pol2Ser5) and enrichment of histone H3 lysine 27 acetylation (H3K27Ac), reminiscent of an enhancer-promoter interaction. The large protein cluster consisted of CTCF, cohesin, and PolSer5 presented a roadblock for the transcription elongation complex, leading to preferential expression of the proximal poly(A) isoform. Conversely, DNA methylation at these same regions prevents CTCF binding; thus, no loop contact forms between the poly(A) sites, and RNA polymerase II can more readily reach the distal poly(A) site. The extent of the interplay between DNA methylation, three-dimensional chromatin structure, and its impact on APA has yet to be fully explored in eukaryotic cells. Here, we postulate that DNA methylation could be modulated during cellular stress response as a potential mechanism upstream of APA, driving the expression of proteostasis-promoting transcripts through CTCF-mediated chromatin loop formation.

To test this hypothesis, we focused on the co-chaperone gene DnaJ heat shock protein family (Hsp40) member B6 (*DNAJB6)*, identified by our analysis as a target of DNA methylation-regulated APA.[19] DNAJB6 functions together with Hsp70 chaperones to prevent protein aggregation and misfolding. Following exposure to HS, we assessed the temporal changes in DNA methylation, *DNAJB6* poly(A) isoform expression, chromatin loop formation, and protein expression. We observed dynamic changes in DNA methylation during HS and recovery at the putative *DNAJB6* APA control

region. The DNA methylation shifts correlated with *DNAJB6* mRNA and protein isoform expression. In addition, we assessed the temporal recruitment of several DNA-binding factors and DNA methylation machinery at this locus in the context of HS to begin unraveling the mechanism for dynamic DNA methylation remodeling during stress response. Altogether, our data illustrate a surprising mechanism connecting the dynamic DNA methylation landscape to chromatin looping and ultimately poly(A) isoform expression during the cellular response to HS.

Results

DNAJB6 isoform expression is mediated by DNA methylation

We previously described a link between DNA methylation, chromatin structure, and APA,[19] where CTCF can bind to DNA demethylated regions between poly(A) sites in a gene to facilitate CTCF/cohesin-mediated chromatin looping, which leads to the physical blockade of RNA polymerase II and subsequent preferential expression of proximal poly(A) isoforms. To gain insight into potential pathways and physiological states where this mechanism may play an important role, we performed gene ontology (GO) analysis on the 546 genes (Table S1). The enriched terms hinted at cellular proteostasis-related functions and processes. The top enriched molecular function terms included protein binding, enzyme binding, cadherin binding, and cytoskeletal protein binding. The top enriched biological processes terms were biological regulation, regulation of protein metabolic process, establishment of localization in a cell, regulation in response to stress, and regulation of protein catabolic process. To explore this potential connection between DNA methylation-regulated APA and proteostasis, we decided to focus on one of the candidate genes with a role in protein turnover, DnaJ heat shock protein family (Hsp40) member B6 (*DNAJB6*).[20–32]

DNAJB6 gene is located on chromosome 7q36.3 and has two annotated isoforms in the reference genome (Figure 1(a)). Previously generated poly(A) sequencing data[19] showed preferential usage of the distal poly(A) site in the DNA methylation-competent HCT116 cells but higher usage of the proximal poly(A) site in the methylation-deficient double-knockout (DKO) cells. By comparing HCT116 cells to DKO, we identified a CpG island (chr7:157,204,349-157,204,587, GRCh37/hg19) between the two poly(A) sites to harbor differential DNA methylation and CTCF/cohesin binding (Figure 1(b)). The poly(A) isoform expression pattern is consistent with what our model of DNA methylation-regulated APA would predict: in the absence of DNA methylation (DKO cells), CTCF and cohesin bind to the CpG island to promote proximal poly(A) isoform expression; in the presence of DNA methylation (HCT116 cells), the lack of CTCF/cohesin binding enables higher distal poly(A) isoform expression. The two mRNA isoforms are translated into two distinct proteins (Figure 1(c) and (d)) that share an identical N-terminal J-domain responsible for interacting with the ATPase domain of Hsp70, as well as an identical G/F domain. The C-termini of both isoforms are serine-rich but differ in length, where the distal isoform sequence contains a nuclear localization signal not found in the proximal isoform (Figure 1(d)).

The two isoforms have been reported to have distinct functions, presumably due to their differential cellular localization. While the proximal DNAJB6 isoform is predominantly cytoplasmic, the distal isoform is primarily nuclear and has been implicated as a tumor suppressor in several malignancies through its nuclear activities in modulating the WNT signaling pathway.[33–35] Both isoforms are capable of suppressing protein aggregation in their respective compartments.[36] As such, the disruption of DNAJB6 activity has been the focus of several diseases characterized by abnormal protein aggregation, including Huntington's disease,[25,37] Parkinson's disease,[38] limb-girdle muscular dystrophy,[39] and Alzheimer's disease.[40] While the expression pattern of DNAJB6 isoforms has been studied in recent years, the mechanism regulating isoform expression is not well understood. Based on our data (Figure 1(b)), the differentially methylated CpG island could be a regulatory sequence involved in APA modulation of *DNAJB6*.

Perturbation of DNA methylation at the APA control region alters *DNAJB6* isoform expression

To confirm differential DNA methylation of this putative APA control region between HCT116 and DKO cells, we preformed targeted bisulfite sequencing across this CpG island. HCT116 cells showed nearly complete methylation of the CpG sites while DKO cells had minimal DNA methylation (Figure 2(a)). *DNAJB6* isoform expression was evaluated by isoform-specific realtime reverse transcriptase (qRT)-polymerase chain reaction (PCR), and consistent with previous poly(A) sequencing data, DKO cells preferentially expressed the proximal poly(A) isoform when compared with HCT116 cells (Figure 2(b)). To test if isoform expression is dependent on DNA methylation, we treated HCT116 cells with the DNA demethylation agent, 5-aza-2′-deoxycytidine (DAC). DAC treatment resulted in the

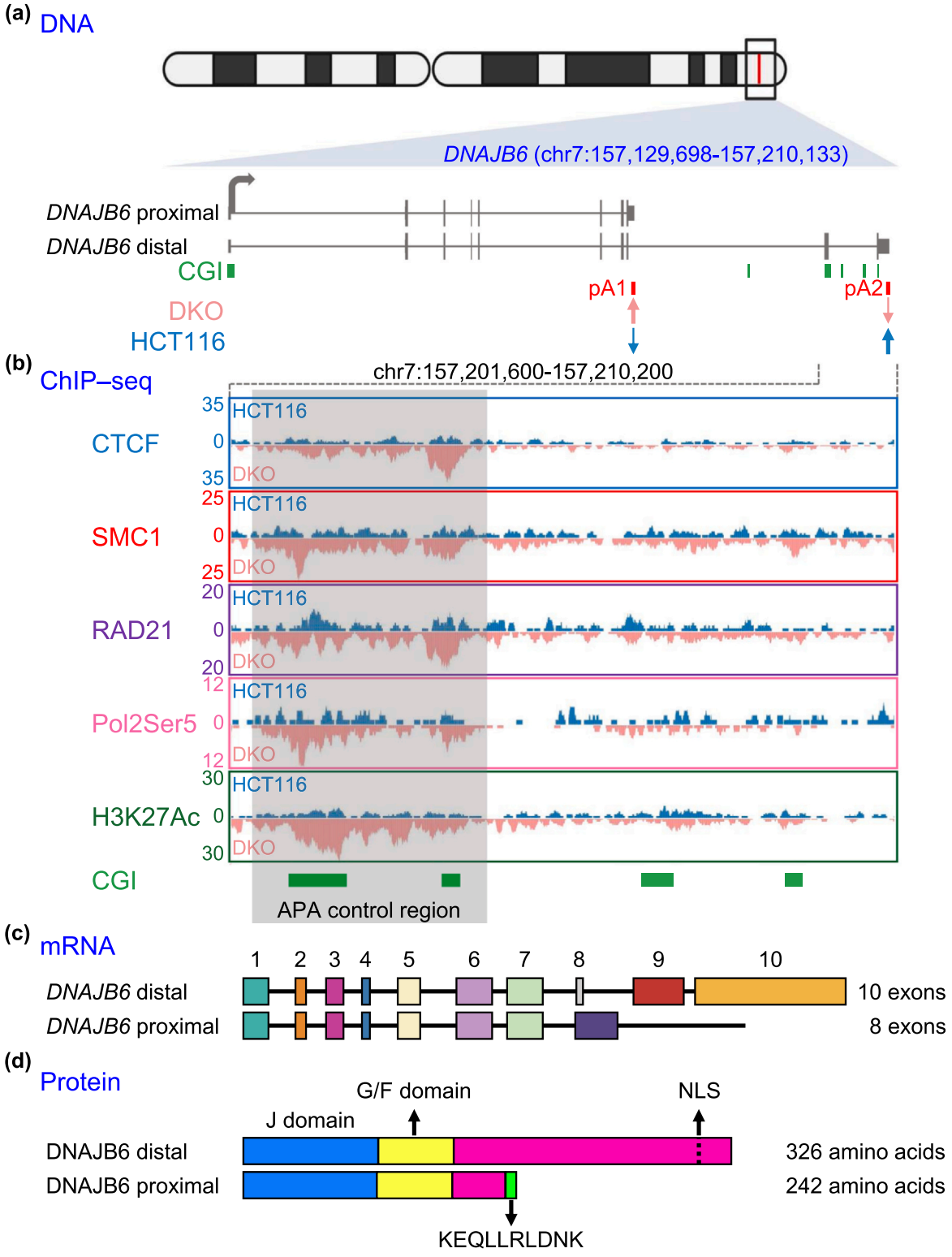

Fig. 1 *DNAJB6* is a target of DNA methylation-regulated APA. (a) Genomic and poly(A) site locations of *DNAJB6*. DKO cells have higher usage of the proximal poly(A) site (pA1), while HCT116 cells have relatively higher usage of the distal poly(A) site (pA2). CGI; annotated CpG islands. (b) UCSC genome capture of ChIP-seq data in HCT116 (blue) and DKO (pink) cells for CTCF, SMC1, RAD21, serine 5 phosphorylated RNA polymerase II (Pol2Ser5), and histone H3 lysine 27 acetylation (H3K27Ac) surrounding the putative *DNAJB6* APA control region. (c) Schematic of mRNA isoforms. (d) Schematic of protein isoforms. Abbreviation used: CTCF, CCCTC-binding factor.

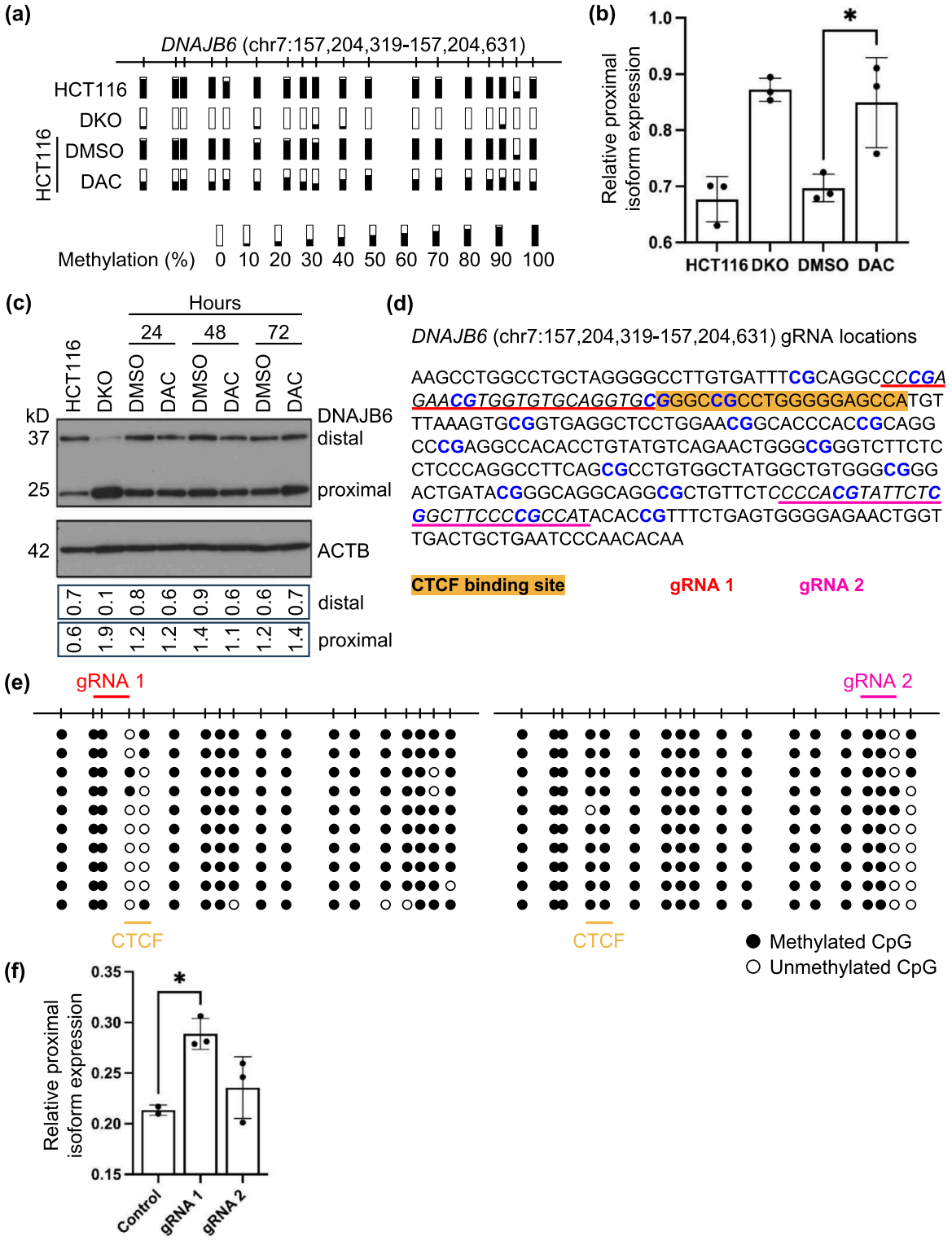
(a)
DNAJB6 (chr7:157,204,319-157,204,631)
HCT116
DKO
HCT116
DMSO
DAC
Methylation (%) 0 10 20 30 40 50 60 70 80 90 100
(b)
Relative proximal isoform expression
1.0
0.9
0.8
0.7
0.6
*
HCT116 DKO DMSO DAC
(c)
Hours
24 48 72
HCT116 DKO DMSO DAC DMSO DAC DMSO DAC
kD
37
25
42
DNAJB6 distal
proximal
ACTB
0.7 0.1 0.8 0.6 0.9 0.6 0.6 0.7 distal
0.6 1.9 1.2 1.2 1.4 1.1 1.2 1.4 proximal
(d)
DNAJB6 (chr7:157,204,319-157,204,631) gRNA locations
AAGCCTGGCCTGCTAGGGGCCTTGTGATTTCGCAGGCCCCGA
GAACGTGGTGTGCAGGTGCGGGCCGCCTGGGGGAGCCATGT
TTAAAGTGCGGTGAGGCTCCTGGAACGGCACCCACCGCAGG
CCCGAGGCCACACCTGTATGTCAGAACTGGGCGGGTCTTCTC
CTCCCAGGCCTTCAGCGCCTGTGGCTATGGCTGTGGGCGGG
ACTGATACGGGCAGGCAGGCGCTGTTCTCCCCACGTATTCTC
GGCTTCCCCGCCATACACCGTTTCTGAGTGGGGAGAACTGGT
TGACTGCTGAATCCCAACACAA
CTCF binding site
gRNA 1
gRNA 2
(e)
gRNA 1
gRNA 2
CTCF
CTCF
Methylated CpG
Unmethylated CpG
(f)
Relative proximal isoform expression
0.35
0.30
0.25
0.20
0.15
*
Control
gRNA 1
gRNA 2

Fig. 2 Methylation status of *DNAJB6* APA control region correlates with poly(A) isoform expression pattern. (a) Amplicon bisulfite sequencing of the putative APA control region in HCT116 and DKO cells, as well as HCT116 cells treated with either DMSO (control) or DAC for 72 h. Each bar represents a single CpG dinucleotide. The methylation level for at least 10 alleles is summarized for each sample. (b) *DNAJB6* proximal poly(A) isoform expression expressed as a fraction of the total *DNAJB6* gene expression in the same cells as in (a). The asterisk denotes statistical significance ($P < 0.05$). (c) Western blot for DNAJB6 protein isoform expression and beta actin (ACTB) loading control in the same cells as in (a). Earlier DAC treatment time points (24 h and 48 h) are also shown. Quantification of the distal and proximal DNAJB6 protein bands were normalized to ACTB and shown underneath the blot image. (d) Design of guide RNAs (gRNAs) used in the dCas9-TET system for targeted DNA demethylation within the *DNAJB6* putative APA control region. Two gRNAs were used, and their respective position within the APA control region is underlined. The predicted CTCF binding site is highlighted in orange. (e) Amplicon bisulfite sequencing of the putative APA control region in HCT116 cells expressing the dCas9-TET system containing sgRNA 1 (left panel) and gRNA 2 (right panel). Black circles represent methylated CpG, and white circles represent unmethylated CpG. Each row represents a single allele. (f) *DNAJB6* proximal poly(A) isoform expression expressed as a fraction of the total *DNAJB6* gene expression in the same cells as in (e). The control cells did not receive any gRNAs. The asterisk denotes statistical significance ($P < 0.05$). Abbreviation used: CTCF, CCCTC-binding factor.

expected decrease in DNA methylation in HCT116 cells (Figure 2(a)) as well as an increase in proximal poly(A) isoform expression (Figure 2(b)). The shift in relative mRNA isoform abundance correlated with a similar trend in protein expression (Figure 2(c)). At baseline, HCT116 cells had both DNAJB6 proximal and distal protein expression while DKO cells had robust proximal protein expression but minimal distal protein expression. With DAC treatment, proximal protein increased in HCT116 cells, mirroring the increase in proximal poly(A) mRNA expression.

While the above results supported that DNA methylation drives *DNAJB6* isoform expression, the genome-wide effects of DAC treatment cannot be ignored as possible confounding factors. Thus, we utilized a dCAS9-mediated epigenome-editing tool[41] to specifically demethylate CpG sites within the putative APA control region. Briefly, a fusion protein (dCAS-TET1-CD) between the catalytic domain of tet methylcytosine dioxygenase 1 (TET1; responsible for active DNA demethylation) and a dead CAS9 was targeted to the putative *DNAJB6* APA control region using two different guide RNA's (Figure 2(d)). Coexpression of the guide RNA (gRNA) with dCAS-TET1-CD in HCT116 cells led to demethylation of specific CpG sites (Figure 2(e)). Isoform-specific RT-PCR revealed that cells expressing gRNA 1 significantly increased their proximal poly(A) isoform expression while cells expressing gRNA 2 did not shift isoform expression patterns significantly (Figure 2(f)). Interestingly, gRNA 1 targeted demethylation of CpG sites that overlap with the predicted CTCF binding motif while gRNA 2 targeted a downstream region that had less impact on isoform expression. Further manipulation of the extent of DNA demethylation within this region by using multiple different gRNAs tiling across this CpG island will help to identify more critical CpG sites in the future. Overall, these results suggest that *DNAJB6* isoform expression is indeed determined by the DNA methylation pattern of this CpG island.

DNAJB6 isoform expression and DNA methylation are regulated in response to HS

Next, we wondered whether any physiological stimuli could promote dynamic changes in *DNAJB6* isoform expression. We selected HS as a physiological stressor, given the known roles of DNAJB6 as a co-chaperone protein involved in maintaining proteostasis. We hypothesized that the APA of *DNAJB6* might be dynamic under conditions where this protein has an important function. To test this, we isolated RNA, DNA, and protein from HCT116 cells at several time points following HS, to capture both the acute and recovery phases. Interestingly, we observed a shift in *DNAJB6* mRNA and protein expression towards the predominantly cytoplasmic proximal isoform immediately after HS, with the pattern persisting for 4 h and recovering back to pre-HS levels at 24 h (Figure 3(a) and (b)).

To test whether DNA methylation was also affected, we preformed targeted bisulfite sequencing on the DNA isolated from these same cells. We observed dynamic changes in the DNA methylation pattern of the APA control region, with almost complete demethylation occurring by 4 h post-HS and recovering to fully methylated status by 24 h post-HS (Figure 3(c)). This quick loss of DNA methylation indicated an active DNA demethylation mechanism, rather than passively losing DNA methylation through cell division. Furthermore, global DNA methylation levels remained mostly unchanged, as indicated by measuring total 5-methylcytosine content using a DNA dot blot (Figure S1(a)), suggesting that the dynamic DNA methylation remodeling is specifically targeted to the *DNAJB6* APA control region.

In our model of DNA methylation-regulated APA, preferential proximal poly(A) isoform expression is achieved by CTCF-mediated chromatin loop formation between the APA control region and distal CTCF binding sites.[19] Leveraging chromatin conformation

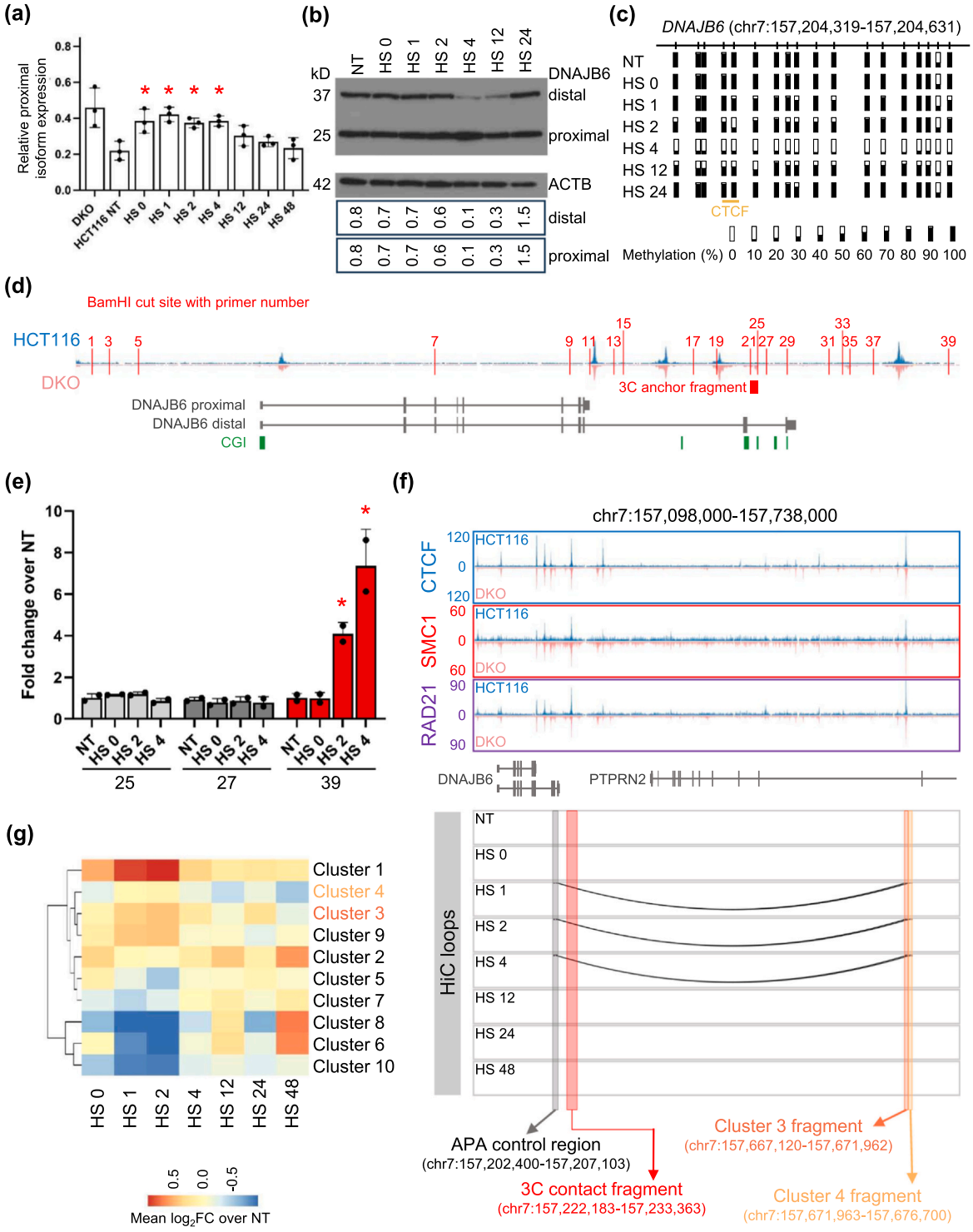
(a)
Relative proximal isoform expression
DKO
HCT116 NT
HS 0
HS 1
HS 2
HS 4
HS 12
HS 24
HS 48
(b)
kD
NT
HS 0
HS 1
HS 2
HS 4
HS 12
HS 24
37
25
42
DNAJB6
distal
proximal
ACTB
distal
proximal
(c)
DNAJB6 (chr7:157,204,319-157,204,631)
NT
HS 0
HS 1
HS 2
HS 4
HS 12
HS 24
CTCF
Methylation (%) 0 10 20 30 40 50 60 70 80 90 100
(d)
BamHI cut site with primer number
HCT116
DKO
3C anchor fragment
DNAJB6 proximal
DNAJB6 distal
CGI
(e)
Fold change over NT
NT
HS 0
HS 2
HS 4
25
27
39
(f)
chr7:157,098,000-157,738,000
CTCF
SMC1
RAD21
HCT116
DKO
DNAJB6
PTPRN2
HiC loops
APA control region
(chr7:157,202,400-157,207,103)
3C contact fragment
(chr7:157,222,183-157,233,363)
Cluster 3 fragment
(chr7:157,667,120-157,671,962)
Cluster 4 fragment
(chr7:157,671,963-157,676,700)
(g)
Cluster 1
Cluster 4
Cluster 3
Cluster 9
Cluster 2
Cluster 5
Cluster 7
Cluster 8
Cluster 6
Cluster 10
Mean log2FC over NT

Fig. 3 Heat shock (HS) induces DNAJB6 poly(A) isoform switching and targeted epigenetic remodeling. (a) *DNAJB6* proximal poly(A) isoform expression expressed as a fraction of the total *DNAJB6* gene expression in DKO, untreated HCT116 (NT), and post-HS HCT116 cells harvested immediately after heat shock (HS 0) and at the indicated time points (HS #, where the number indicates hours post-HS). Asterisks identify HS samples that are statistically different from untreated (NT) HCT116 ($P < 0.05$). (b) Western blot for DNAJB6 protein isoform expression and beta actin (ACTB) loading control in the same HCT116 cells as in (a). Quantification of the distal and proximal DNAJB6 protein bands were normalized to ACTB and shown underneath the blot image. (c) Amplicon bisulfite sequencing of the APA control region in the same cells as in (b). Each bar represents a single CpG dinucleotide. The methylation level for at least 10 alleles is summarized for each sample. (d) Schematic of the 3C assay fragments (defined by *Bam*HI cut sites marked as red vertical lines) overlayed on top of the CTCF ChIP-seq data in HCT116 (blue) and DKO (pink) cells. The numbers correspond to the PCR primers used in the 3C assay and are listed in Table S4. The anchor fragment containing the APA control region is noted in red. (e) Fold enrichment of 3C fragment amplification in post-HS HCT116 cells (HS #, where the number indicates hours post-HS) over untreated HCT116 cells (NT) for primers 25 (light gray bars), 27 (dark gray bars), and 39 (red bars). The asterisk identifies HS 4 as statistically different from NT (adjusted $P < 0.05$). (f) UCSC genome browser view showing the *DNAJB6* APA control region and the two interacting genomic fragments detected by Hi-C. ChIP-seq data for CTCF, SMC1, and RAD21 in HCT116 (blue) and DKO (pink) are shown along with Hi-C loops originating from the *DNAJB6* APA control region in untreated HCT116 (NT), and post-HS HCT116 cells harvested immediately after heat shock (HS 0) and at the indicated time points (HS #, where the number indicates hours post-HS). The loop contact fragment discovered in the 3C experiment from (e) is also labeled. Genomic coordinates are from GRCh37/hg19. (g) Heatmap of mean log2 fold change (Log_2FC) of loop strengths over untreated HCT116 (NT) for the 10 dynamic loop clusters in Figure S1(c). Cluster 3 and 4 contained the *DNAJB6* interacting fragments chr7:157,667,120-157,671,962 and chr7:157,671,963-157,676,700, respectively. Abbreviation used: CTCF, CCCTC-binding factor; PCR, polymerase chain reaction.

capture (3C) assay, we detected several distal genomic regions that interact with the *DNAJB6* APA control region as a function of differential DNA methylation (Figures 3(d) and S1(b)). Of note, chromatin contacts between the APA control region and *Bam*HI fragments assayed by primers 25, 27, and 39 were the most enriched in DKO cells (Figure S1(b)), nominating these as regions of interest to test in the HS time course. At 2-hour and 4-hour post-HS, we observed increased interaction between the APA control region and *Bam*HI fragment assayed by primer 39 (Figure 3(e)). This fragment (chr7:157,222,183-157,233,363, GRCh37/hg19) is about 18 kb downstream from the APA control region, and it contains a clear CTCF binding site, as previously assayed by ChIP-seq (Figure 3(d)). The 3C results strongly suggested that a CTCF-mediated chromatin loop was formed upon DNA demethylation of the APA control region, consistent with our working model. Because the 3C-based detection of chromatin loops is limited by user-defined regions, we performed Hi-C-seq across the HS time course to investigate the local and global chromatin architecture changes more thoroughly during HSR.

The Hi-C analysis identified two adjacent genomic fragments located approximately 460 kb downstream from the APA control region (Figure S1(c)). These fragments formed chromatin loop contacts with the APA control region starting at 1-hour post-HS and resolving by 12-hour post-HS (Figure 3(f)). While we did not detect interaction with the 3C contact fragment, due to the inherent resolution limit of the Hi-C technique, we noted that the dynamic behavior of these Hi-C-identified distal interacting fragments was similar to that observed for the 3C loop contact fragment. Importantly, all 3 interacting fragments harbored strong concurrent binding of CTCF, SMC1, and RAD21 in HCT116 cells (Figure 3(f)). Previously, Hi-C analysis was utilized to assess global chromatin changes during acute HS and found that topologically associating domains and compartment structures stayed mostly unchanged in human and *Drosophila*.[42] However, our findings at *DNAJB6* suggest that dynamic chromatin structure changes over time following HS may have been overlooked previously. Thus, we further analyzed our Hi-C data for dynamic looping interactions across the HS time course and could segregate the looping interactions into 10 dynamic patterns (Figure S1(d)). The two APA control region-interacting fragments fell in cluster 3 (57,293 loops) and cluster 4 (45,489 loops), both of which demonstrated increased interaction strengths at 1-hour and 2-hour post-HS (Figure 3(g)). We annotated these looping interactions (Table S2) and anticipated that, with additional parallel epigenetic and transcriptomic data, we could identify other genes regulated similarly to *DNAJB6* during HSR.

Collectively, these observations demonstrated that HS stress triggered a rapid change in *DNAJB6* poly(A) isoform expression pattern and invoked targeted DNA demethylation at the APA control region as part of the regulation. Isoform switching appeared to precede complete DNA demethylation, suggesting that additional signal transduction must be involved during the early phase of HSR to modulate APA and recruit DNA methylation modifiers for a sustained transcriptional countermeasure to this cellular stress.

Identification of factors mediating DNA methylation-regulated APA during cell stress

We speculated that additional factors participated in the HS-induced APA. The CTCF binding motif predicted in mediating DNA methylation-regulated APA at *DNAJB6* is only 19 bp in a 239 bp CpG island (Figure 4(a)), but the DNA methylation changes that occurred during

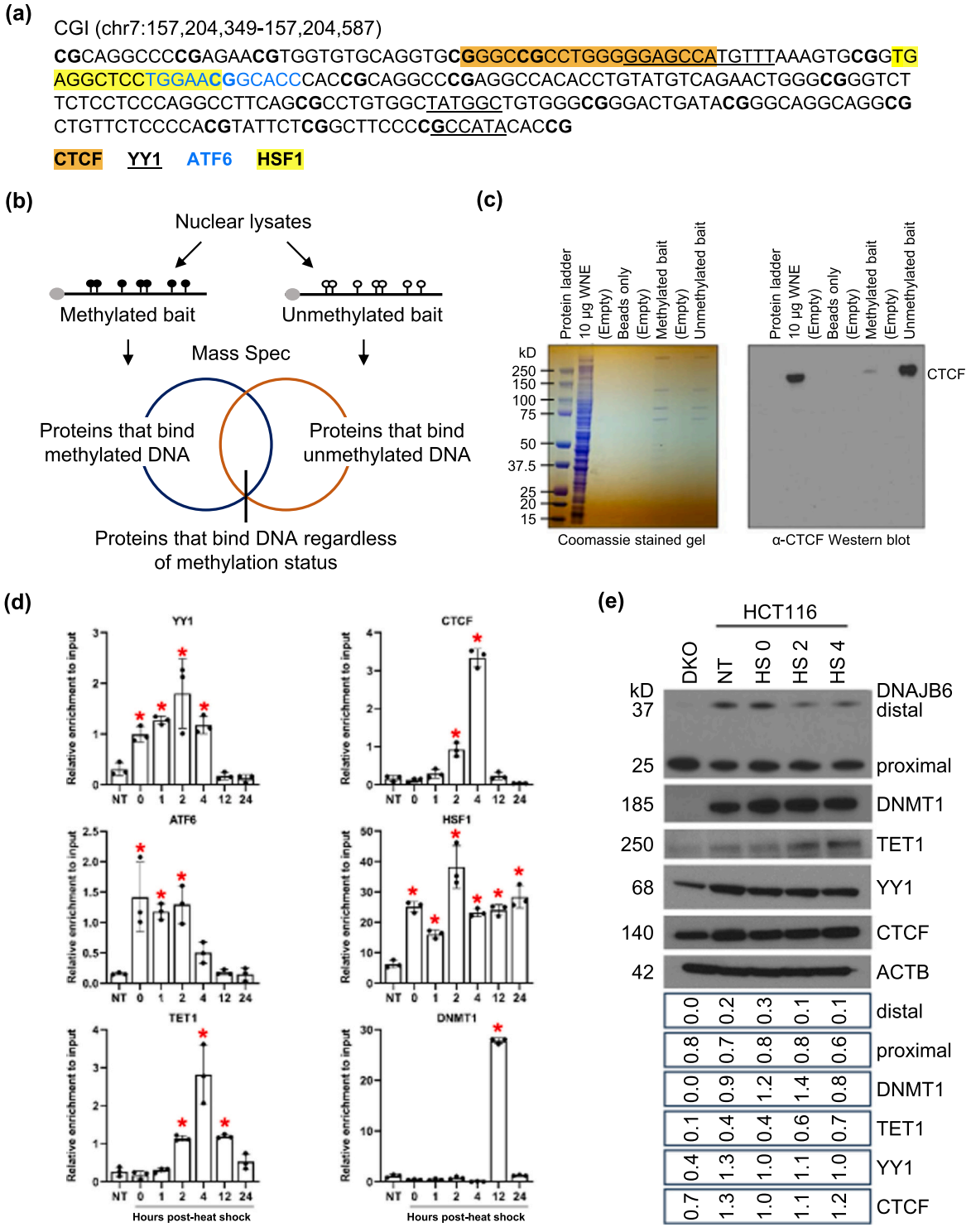

Fig. 4 Transcription factors and DNA methylation modulators bind to the *DNAJB6* APA control region. (a) Annotation of the CpG island (CGI) sequence in the APA control region. Predicted binding sites for CTCF (highlighted in orange), YY1 (underlined), ATF6 (blue letters), and heat shock factor 1 (highlighted in yellow) are marked. (b) Workflow of DNA pulldown experiment. (c) Images of DNA pulldown cell lysates resolved on acrylamide gels and stained with Coomassie (left panel) and probed with anti-CTCF antibody (right panel). Beads only, elute from reactions without nuclear extracts; Methylated bait, elute from reactions containing methylated bait; unmethylated bait, elute from reactions containing unmethylated bait. (d) ChIP-qPCR in untreated HCT116 cells (NT) and post-heat shock (HS) HCT116 cells immediately after HS(0) and at the indicated number of hours post-HS. Asterisks identify HS samples that are statistically different from untreated (NT) HCT116 ($P < 0.05$). (e) Western blot for DNAJB6 protein isoforms, DNMT1, TET1, YY1, CTCF, and ACTB loading control in DKO, untreated HCT116 (NT), and post-HS HCT116 cells at the indicated time points. Quantification of the protein bands was normalized to ACTB and shown underneath the blot image. Abbreviations used: CTCF, CCCTC-binding factor; DNMT1, DNA methyltransferase 1; TET1, tet methylcytosine dioxygenase 1; WNE, whole nuclear extract; YY1, Yin Yang 1; qPCF, realtiem PCR.

HSR encompassed the entire CpG island. Therefore, we performed DNA pulldown followed by mass spectrometry to discover additional proteins involved in mediating the observed DNA methylation and chromatin structure changes. We used the entire CpG island as the DNA bait and performed the experiment with either methylated or unmethylated baits to identify both DNA methylation-sensitive and insensitive binding proteins (Figure 4(b)). As a control, we probed the eluted proteins for CTCF and saw robust CTCF enrichment in the reaction containing the unmethylated bait (Figure 4(c)). After filtering out non-specific and low abundance proteins from replicate experiments, we identified 139 candidate binding proteins for the *DNAJB6* APA control region (Table S3). A small subset of these proteins, including methyl-CpG binding domain protein 2 (MBD2) and E3 ubiquitin-protein ligase UHRF1 (UHRF1), showed DNA methylation-sensitive binding of the DNA baits, but the majority appeared to bind the DNA baits regardless of methylation status. To help prioritize for validation and functional studies, we annotated the protein list using GO terms and manually curated proteins with sequence-specific DNA binding (GO:0043565) for known functions in epigenetics, cell stress, and chromatin looping.

Based on the above criteria, we focused on Yin Yang 1 (YY1). YY1 is a constitutively expressed transcription factor known to contribute to chromatin loop formation, similarly to CTCF, in the context of promoter-enhancer interactions.[43] Cobinding and crosstalk between CTCF and YY1 have been reported across a variety of cell types and developmental stages, especially in the neural lineage.[44–46] Sequence analysis of the APA control region identified three putative YY1 binding sites, one of which directly overlapped the CTCF motif (Figure 4(a)). Interestingly, this analysis also revealed potential binding sites for ATF6 and HSF1, both of which have well established roles in signal transduction during HSR and UPR,[47–50] in this same genomic region. Because the DNA pulldown experiment was limited to untreated conditions, we wanted to explore in greater detail the DNA-binding dynamics of CTCF, YY1, ATF6, and HSF1, as well as DNA methylation regulators, DNA methyltransferase 1 (DNMT1) and TET1. To this end, we preformed chromatin immunoprecipitation (ChIP) on HCT116 cells following HS treatment and observed immediate binding of ATF6, HSF1, and YY1 at the APA control region (0-hour time point in Figure 4(d)), concurrent with the increase in proximal poly(A) isoform expression (Figure 3(a)). However, there appeared to be slight differences in the binding dynamic of these three transcription factors; HSF1 localization persisted throughout the entire time course, ATF6 binding tapered off by 4-hour post-HS, while YY1 binding peaked at 2-hour post-HS. This observed pattern likely resulted from differences in how these transcription factors operate during stress response; HSF1 activation is achieved through homotrimer formation upon release from molecular chaperone proteins[51,52] and *via* direct thermo-sensing,[53] soluble ATF6 is released from ER by proteolysis so that it can translocate into the nucleus,[54] and finally, ATF6 and YY1 coactivate transcription at ER stress element-containing promoters during UPR.[55]

We sought to knock out each transcription factor to determine their role in *DNAJB6* APA regulation. CRISPR editing of YY1 did not yield any viable cells, while clones with complete ATF6 knockout (KO) could not be isolated (Figure S2(a) and (b)). Similarly, shRNA-mediated knockdown of YY1 and ATF6 significantly reduced colony formation (Figure S2(c)); any surviving cells had minimal reduction in YY1 (Figure S2(d)) or ATF6 (Figure S2(e)). These data suggested that YY1 and ATF6 were essential for HCT116 cell survival, and a more targeted strategy will be needed to probe their functions in APA control. In contrast, HSF1 knockout cells were viable (Figure S2(f)) and demonstrated a delay in *DNAJB6* APA isoform shift upon HR when compared with parental HCT116 cells (Figure S2(g)). However, the HSF1 KO cells also showed a delay in activation of HSP70 (Figure S2(h) and (i)), a marker for HSR, thus complicating the interpretation of the phenotype.

Next, we detected TET1 recruitment to the APA control region starting at 2-hour post-HS and peaking at 4-hour, coinciding with the near complete demethylation of this region seen by targeted bisulfite sequencing (Figure 3(c)). TET1 is one of three enzymes responsible for active DNA demethylation in mammalian cells, converting 5-methylcytosines to 5-hydroxy cytosine, 5-carboxyl cytosine, and 5-formyl cytosine in a stepwise fashion.[56–58] Therefore, its localization to the APA control region provided a molecular explanation for the rapid DNA demethylation observed at this region. It is worth noting that the bisulfite sequencing results likely underestimated the actual decrease in 5-methylcytosine level at early time points since bisulfite sequencing could not distinguish between methylated and hydroxymethylated cytosines.

Tracking nicely with the methylation status of its binding site (Figure 3(c)), CTCF was also detected here starting at 2-hour post-HS and disappearing by the 12-hour post-HS time point (Figure 4(d)). Finally, as the cells recovered from the heat stress and restored *DNAJB6* proximal poly(A) isoform expression back to homeostatic level, DNMT1 was found at this region to facilitate DNA re-methylation (Figure 4(d)). Next, we

probed for these proteins to determine if their dynamic association with the APA control region was driven by their overall levels (Figure 4(e)). Interestingly, only TET1 protein level seemed to have increased during this time course. While we were not aware of published reports on HS inducing TET1 transcription, scanning the TET1 promoter sequence identified a HSF1 motif (−264 bp from transcription start site) and two ATF6 motifs (−269 bp and +43 bp from transcription start site), raising the possibility that TET1 expression could be stimulated in response to cellular stress.

Discussion

Altogether, our data suggested that the *DNAJB6* APA control region contains sequence elements that allow for binding and integration of stress-sensing transcription factors (HSF1 and ATF6) to quickly increase *DNAJB6* proximal poly(A) isoform expression during HSR and produce the corresponding cytoplasmic protein isoform capable of activating HSP70 and suppressing protein aggregate.[59] Our observations suggested a model where the transcriptional coregulator, YY1, also binds to this same region to facilitate isoform switching. TET1 is then recruited to rapidly demethylate the APA control region, which enables CTCF binding and the ensuing chromatin loop formation. Based on our prior work, this CTCF-mediated chromatin looping can further enforce proximal poly(A) mRNA expression, thus ensuring reliable proximal protein production to support cell needs. As the cells recover from HS, the transcription factors terminate their tenure at the APA control region, DNMT1 is recruited to remethylate the DNA, and the *DNAJB6* APA rheostat is reset.

Combinatorial transcription factor binding is thought to contribute to the evolutionary stabilization of DNA regulatory regions; therefore, this co-occurrence of YY1, ATF6, HSF1, and CTCF binding, overlaying the dynamic DNA methylation scenery, highlights the *DNAJB6* APA control region as an important and tuneable regulatory element of gene expression, akin to a gene promotor. Moreover, the 3D chromatin loop formation and the enrichment of histone H3 lysine 27 acetylation and serine 5 phosphorylated RNA polymerase II at this same region strikingly resemble classical enhancer-promoter interactions that regulate transcription activity of single poly(A) site genes. Recently, enhancers have been shown to regulate APA in addition to modulating the total transcriptional output of multi-UTR genes.[60] In this study, perturbations of YY1, CTCF, and cohesin complex components altered the cleavage and polyadenylation activity of a reporter system for *PTEN* APA. Thus, we surmise that the distal interacting fragments detected by 3C and Hi-C potentially contain enhancer elements that further contribute to the fine-tuning of *DNAJB6* APA. While there is robust literature on stress-induced gene activation and silencing, our findings here represent a novel example of stress-induced transcriptome modulation, where transcription factors, DNA methylation, and chromatin architecture converge to achieve a necessary poly(A) isoform expression pattern.

Our observations also raised several important questions that warrant further investigation. First, how universal is this mechanism during different types of cellular stress response? We speculate that stressors that elicit overlapping signal transduction pathways might induce similar changes in chromatin and isoform expression in *DNAJB6* and other potential targets. For instance, drugs that cause ER stress, such as tunicamycin and thapsigargin, are known to activate ATF6 and can potentially trigger similar APA and chromatin changes described in this study.

Second, what are the genes subjected to this type of APA regulation? While we came upon *DNAJB6* through our prior work investigating the function of gene body DNA methylation, HS offers an excellent context to identify physiologically relevant APA globally using genomic approaches. Related to this, HSF1 binding to the D*NAJB6* APA control region was longer than what has been reported at canonical promoter regions. This phenomenon may be specific to APA control and potentially regulated by post-translational modifications of HSF1.[61] Our Hi-C data identified many dynamic loop interactions that behaved similarly to the *DNAJB6* APA control region. Combining these results with additional epigenetic, transcription factor binding, and poly(A)-seq data should help enumerate other genes regulated in an analogous manner.

Third, the swift DNA methylation changes and the sequential binding of transcription factors preceding methylation changes in the HS time course present an exquisite opportunity for investigating stress-induced DNA methylome remodeling. An obvious question is whether YY1 facilitated the recruitment of TET1. It has been reported that YY1 has DNA methylation sensitivity, but the results from the DNA pulldown experiment indicated that it can bind regardless of DNA methylation. While we were unable to achieve YY1 depletion to test this hypothesis, it is still tempting to speculate on the necessity of YY1 binding in facilitating the recruitment of DNA demethylation machinery and subsequent CTCF binding. Future studies on the global chromatin occupancy of these factors and associated chromatin contexts, including nucleosome positioning,

under dynamic conditions, will be important for further understanding of this gene regulation mechanism.

Finally, it is worth noting that *DNAJB6* poly(A) isoforms can also be alternatively spliced to generate different 3′ coding regions and 3′ UTR. Alternative splicing and APA are often coupled during mRNA processing. However, delineating the relative contribution of alternative splicing and APA in regulating isoform expressions or how each process impacts the other is beyond the scope of this current study, but it will be highly interesting to investigate in the future.

Conclusions

Our results showed that the increase in *DNAJB6* proximal poly(A) isoform expression is regulated during HS through recruitment of HSF1, ATF6, YY1, and TET1 to the *DNAJB6* APA control region. Subsequently upon DNA demethylation, CTCF binding to this region facilitated chromatin loop contact formation to reinforce the isoform expression pattern. As cells recover, the transcription factors and chromatin loops resolve to return DNAJB6 isoform expression to base line.

Materials and methods

Cell culture

HCT116 and HEK-293 cells were obtained from the ATCC. DNMT1 and 3b DKO cells were obtained from the laboratory of Dr Bert Vogelstein.[62] HCT116 and DKO were cultured in McCoy's 5a Medium Modified (Thermo Fisher Scientific) supplemented with fetal bovine serum (FBS) (Corning) to a final concentration of 10%. The HEK-293 cells were cultured in Eagle's Minimum Essential Medium (Thermo Fisher Scientific) supplemented with FBS (Corning) to a final concentration of 10%. All cells were kept in an incubator at 37 °C with 5% CO_2. For HS, cells were incubated at 43 °C for 1 h. Cells were harvested immediately after the 1-hour incubation for the time 0 time point and at 1, 2, 4, 12, 24, and 48 h after recovery at 37 °C. DAC treatment was performed as described previously.[19]

dCas-directed DNA demethylation

We established HCT116 cell lines that expressed the dCas9-TET demethylation system as described previously.[41] First, lentivirus containing either control or the DNAJB6 gRNA expression construct (VectorBuilder) was made using HEK-293 cells, following the standard LipoD293 transfection protocol (SignaGen Laboratories), with the envelope (pCMV-VSV-G, AddGene) and packaging (psPAX2, AddGene) plasmids in a 2.5:1 ratio. At 48 h post transfection, lentivirus-containing media were collected from the HEK-293 cells, filtered, and added to the HCT116 cells in the presence of 8 μg/mL polybrene (Sigma-Aldrich). Lentivirus-containing media were replaced after 24 h with regular culture media supplemented with 10% FBS, and infected cells were selected using 1 μg/mL puromycin (Sigma-Aldrich) for 48 h. Following selection, the HCT116 cells were transfected with both pdCas9-Tet1-CD (Addgene) and pcDNA3.1-MS2-Tet1-CD (Addgene) plasmids using Lipofectamine 2000 (Life Technologies) according to the manufacturer's instructions. Cells were harvested 2 days post transfection for RNA and genomic DNA extraction.

ChIP

ChIP was performed using the Magna ChIP A/G kit (Sigma-Aldrich) following the manufacturer's protocol. The antibodies and their respective dilutions are as follows: CTCF antibody (Cell Signaling Technology #2899) at 1:25 dilution, YY1 antibody (Cell Signaling Technology #46395) at 1:50 dilution, ATF6 antibody (Cell Signaling Technology #65880) at 1:50 dilution, TET1 antibody (ThermoFisher #61443) at 1:25 dilution, HSF1 antibody (Novus #NBP2-42206V) at 1:50 dilution, and DNMT1 antibody (Sigma-Aldrich #D4692) at 1:50 dilution.

DNA pulldown

The DNA pulldown protocol was adapted from the previously published procedure[63] with a few minor changes. DNA probes (chr7:157,204,244-157,204,652, GRCh37/hg19) spanning the APA control region in *DNAJB6* were generated using PCR (EpiMark-HS-TAQ, New England Biolabs), where one set of reactions used a 5-methylcytosine-containing dNTP mix (methylated probes) and the other set used the dNTP mix without methylated bases (unmethylated probes). Terminal transferase (New England Biolabs) was used to add a biotinylated dUTP tail. DNA probes were incubated with nuclear lysates from untreated HCT116 cells. DNA/protein complexes were extracted using streptavidin magnetic beads, and a bead-only control was included as a third reaction. Eluted proteins from each reaction were resolved using sodium dodecyl sulfate polyacrylamide gel electrophoresis. The DNA pulldown experiment was performed in biological duplicates.

The gel was stained with Coomassie Blue and subjected to in-gel protein digestion for liquid chromatography-mass spectrometry sample preparation. Briefly, each lane in the gel was divided into smaller pieces, washed (50% ethanol), destained (5% acetic acid), dehydrated (acetonitrile), dried, reduced, alkylated, and then digested with trypsin (5 μL of 10 ng/μL trypsin in 50 mM HCO_3) overnight at room temperature. The peptides were extracted from polyacrylamide with two aliquots of 30 μL of 50% acetonitrile with 5% formic acid. The aliquots were combined and evaporated to < 10 μL in Speedvac and then resuspended in 1% acetic acid to a final volume of 30 μL for liquid chromatography-mass spectrometry analysis using a ThermoScientific Fusion Lumos mass spectrometry system. The data were analyzed by using all CID spectra collected in the experiment to search against the human SwissProt database and the sequences of Human HIF-2-alpha (accession Q99814) using the program Sequest. The search results were further validated with Scaffold (Scaffold_4.7.2, Proteome Software Inc).

Within each biological replicate, proteins with < 10 spectral counts were filtered out. Next, only those proteins with a ≥5-fold enrichment of spectral counts over bead control were considered positive. Finally, 139 proteins were reproducibly identified in both biological replicates (Table S3) and further annotated as chromatin binding (GO:0003682), transcription factor binding (GO:0008134), DNA-binding transcription factor binding (GO;0140297), sequence-specific DNA binding (GO:0043565), DNA secondary structure binding (GO:0000217), or transcription regulator activity (GO:0140110) using g:Profiler.[64]

Targeted bisulfite sequencing

DNA was bisulfite converted using the EZ DNA methylation-gold kit (Zymo #D5006). *DNAJB6* loci of interest were amplified using the primers listed in Table S4. Amplicons were resolved on 1% agarose gel by gel electrophoresis and purified using the QiaQuick Gel Extraction Kit (QIAGEN #28706). Purified PCR product was cloned into the TOPO TA Vector and transformed into OneShot TopTen Chemically Competent Escherichia coli cells (Thermo Fisher Scientific #K457540). Alleles were analyzed using BISMA[65] after Sanger sequencing.

Quantification of poly(A) isoform expression by qRT-PCR

Total RNA was extracted by AllPrep kit (Qiagen). Oligo-dT[16] primer was used to convert 1 μg of total RNA into cDNA using Superscript III reverse transcriptase (Thermo Fisher #18080093), and 40 ng of cDNA was used for each realtiem PCR reaction with QuantiTect SYBR green reagent (QIAGEN #204143). PCR primers for specific poly(A) isoforms are listed in Table S4. Relative isoform expression for *DNAJB6* was calculated as the distal isoform level divided by the total gene level. Results were calculated from biological triplicates that were assayed by technical triplicate PCR reactions, and statistical significance was determined using ordinary one-way Analysis of Variance with multiple comparisons correction in GraphPad Prism 9.0.0.

Chromatin conformation capture (3C)

The 3C was performed following previously optimized protocols[19,66] with minor changes. In brief, a total of 10^7 cells were harvested with trypsin, washed, and resuspended in 9.5 mL PBS. The samples were cross-linked in 1% formaldehyde for 10 min at room temperature with rotation. Nuclei were extracted by incubating cells on ice for 10 min using 5 mL cold lysis buffer [10 mM Tris-HCl, pH 7.5; 10 mM NaCl; 5 mM $MgCl_2$; 0.1 mM EGTA; 1X complete protease inhibitor (Roche #11836145001)]. Pelleted nuclei were resuspended in 0.5 mL 1.2× restriction enzyme buffer with 0.3% SDS and incubated for 1 h at 37 °C while shaking at 900 rpm, followed by the addition of Triton X-100 to 2% final concentration and incubated for 1 h at 37 °C while shaking. A total of 400 U of *Bam*HI (NEB #R1036S) was added, and cells were incubated overnight at 37 °C with shaking. SDS was added to a 1.6% final concentration, and samples were incubated at 65 °C for 20 min with shaking. Ligation of the digested DNA was carried out by adding 6.125 mL of 1.15x ligation buffer (10X: 660 mM Tris-HCl, pH 7.5; 50 mM DTT, 50 mM $MgCl_2$, 10 mM ATP) and adding Triton X-100 to a final concentration of 1%, followed by incubation for 1 h at 37 °C with gentle shaking. Samples were incubated with 100 U of T4 DNA ligase (NEB #M0202S) for 4 h at 16 °C followed by 30 min at room temperature. Samples were then decross-linked overnight at 65 °C with 300 μg proteinase K (Invitrogen #25530049), followed by incubation with 300 μg RNase A (Invitrogen #EN0531) for 30 min at 37 °C. DNA was purified using phenol/chloroform extraction and resuspended in 150 μL of 10 mM Tris pH 7.5. DNA was quantified using one primer adjacent to the *Bam*HI cut site in each distal fragment and another one within the anchor region (Table S4) by SYBR green real-time quantitative PCR on the Roche LightCycler® 96 on 50X diluted 3C DNA and serial dilutions of reference DNA of known concentration using internal primer sets that do not amplify across *Bam*HI cut sites.

Hi-C-seq assay and sequencing data analysis

Sample preparation for the Hi-C-seq experiment was done following the Arima-Hi-C workflow (Arima #A510008). Ten million cells per sample were cross-linked for each reaction, and two biological replicates were assayed for each HS time point and the no treatment control. A minimum of 500 million 150 bp pair-end reads per sample was sequenced. The reads were trimmed to 40 bp to maximize alignment prior to following the Hi-C data preprocessing (https://github.com/JinLabBioinfo/DeepLoop/tree/master/preprocessing) workflow towards application of HiCorr[67] and DeepLoop.[68] Preprocessing included deduplication and mapping of read pairs to Arima fragment pairs using the Arima fragment bed. We then applied HiCorr, in the "Arima" mode, to identify bias-corrected 5-kb anchor loop files from *cis–trans* fragment read pairs. Following HiCorr, the number of *cis* 2-Mb contacts was computed for each sample to determine which pre-trained DeepLoop model best suited the data. Given that the average number of *cis* 2-Mb contacts was ~200 M, we applied the next closest 250 M model.

Downstream loop analysis was performed in R v4.3.1. Following the prediction, the loops in each sample were sorted based on loop strength, and the top 300,000 loops per time point were found. Towards identification of dynamic loop changes over time post-HS, the union of the top 300,000 loops across all samples was found (total 599,147) and extracted per sample. For each sample, loop sets were then normalized (division by sum), and the log2FC with respect to the untreated sample was computed. To reduce the dimensionality of the data, loops that demonstrated < 5% variance across all time points or a total absolute log2FC < 1.5 were excluded. The final data were comprised 381,291 enriched loops and was visualized as a heatmap (pheatmap,[69] v1.0.12). Loops (heatmap rows) were then clustered based on their dynamic behavior over time using K-Means clustering (factoextra,[70] v1.0.7). Ten clusters of dynamic loops were resolved, and the clusters containing an interaction originating from the *DNAJB6* APA control region were identified in Clusters 3 (57,293 loops) and 4 (45,489 loops). These interactions were annotated using HOMER[71] v4.11. Enriched *DNAJB6* APA control region interactions were visualized using UCSC Genome Browser[72] as big interact files.

Western blot

Cells were lysed in 3% SDS in 10 mM Tris pH = 7.5 by pipetting, then centrifuged through a Qiashredder column (Qiagen #79656). Protein concentrations were determined by BCA assay (Thermo Fisher Scientific #23225). A total of 10 μg of cell lysate per sample were resolved on sodium dodecyl sulfate polyacrylamide gel electrophoresis in NuPAGE reducing sample buffer (Thermo Fisher Scientific #NP0001) using the Novex system at 120 V for 1 h. Proteins were transferred to PVDF membrane using a 1X transfer buffer (Thermo Fisher Scientific #NP0006-1) with 10% methanol at 30 V for 3 h at 4 °C. Membranes were blocked in 10% nonfat dairy milk in 1X TTBS (25 mM Tris-HCl, 155 mM NaCl, 0.1% Tween 20) overnight at 4 °C. Membranes were incubated either at room temperature for 2 h or overnight at 4 °C with primary antibodies in 5% milk in 1X TTBS at the following concentrations: DNAJB6 (Abcam #ab198995; 1:1000), CTCF (Cell Signaling Technology #2899; 1:1000), YY1 (Cell Signaling Technology #46395; 1:1000), DNMT1 (Sigma-Aldrich #D4692; 1:1000), TET1 (Thermo Fisher Scientific #61443; 1:500), ATF6 (Novus #NBP2-80583; 1:1000), HSF1 (Cell Signaling #12972; 1:1000), GAPDH (Cell Signaling #2118; 1:1000), and HSP70 (Santa Cruz #sc-66048; 1:1000). Rat and mouse secondary antibodies were used at 1:5000 in 5% milk in 1X TTBS with 1.5-hour incubation at room temperature. ACTB primary antibody (Sigma-Aldrich #A3584) was used at 1:10,000 dilution in 5% blocking buffer with a 1-hour incubation at room temperature. Membranes were washed five times for 5 min each in 1X TTBS at room temperature after primary and secondary antibody incubations. Membranes were exposed to film following incubation with ECL Plus (Thermo Scientific #32132). Blot images were loaded into MATLAB, and a global mean-based threshold was applied to segment bands from the background. Binary images of segmented bands were exported. Blot images and masks were then loaded into ImageJ. The masks were set as binary images by selecting Image > Adjust > Threshold and clicking Apply. Segmented bands were enumerated and measured in the mask using Analyze > Analyze Particles and selecting "Display results," "Add to [ROI] Manager," and "Exclude on edges." The blot image was then selected, and "Measure" in the ROI Manager was selected, producing area and mean intensity measurements for each band in the blot, which were exported to csv files. CSV files were loaded into Microsoft Excel. Band integrated density was calculated by multiplying band area by band mean intensity. For each experimental band, relative expression by linear fold change was calculated by dividing the integrated density of the experimental band by the control band (ACTB).

CRISPR-Cas9 genome editing

Three independent sgRNAs were designed to target the coding regions of YY1, HSF1, and ATF6 genes (sgRNA

sequences in Table S5). The sgRNA sequences were cloned into the lentiCRISPR-v2 vector (Addgene #52961), and the constructs were verified by sequencing. HCT116 cells were transfected with lentiCRISPR-V2 expressing sgRNA using Lipofectamine 3000 (Thermo Fisher Scientific #L3000015). Cells were then selected by puromycin (1 μg/mL). The editing efficiency of the pooled cells was determined using the T7 endonuclease I (T7EI) assay (NEB #E3321S). Briefly, genomic DNA from transfected cells was amplified using primers flanking the sgRNA-targeted regions (Table S4). For T7EI digestion, amplified PCR products were denatured at 95 °C for 5 min and slowly cooled to room temperature to allow formation of heteroduplex DNA. The annealed products were incubated with 0.5 μL T7EI for 30 min at 37 °C, and the digested DNA was separated on 2% agarose gels. For cell pools with evidence of editing, single-cell clones were selected using limiting dilution cloning in 96-well plates. Individual clones were further expanded and confirmed by Western blot.

shRNA transfection

GIPZ Lentiviral constructs for YY1, HSF1, ATF6, and nontargeting shRNA control were obtained from MD Anderson Functional Genomics Core. The sequences of shRNAs are listed in Table S5. The transfection of shRNA-expression plasmids into the cells was performed using Lipofectamine 3000 reagent (Thermo Fisher Scientific #L3000015) in accordance with the manufacturer's protocol. Cells were transfected with shRNA for 48 h, then selected by puromycin (1 μg/mL) for 3 days before proceeding to subsequent experiments.

Colony formation

Following transfection with shRNA for 48 h, cells were trypsinized and counted. A total of 1×10^4 cells were seeded into 35-mm dishes and cultured in puromycin-containing media for 10 days. Cells were fixed with 100% methanol for 0.5 h and stained with 0.1% crystal violet for 0.5 h. Colonies on triplicate plates were counted.

Funding and support This work was supported by the National Institutes of Health [R01 CA1230033 to A.H.T., F32 CA260774 to E.E.F.]. Funding for open access charge: UT MD Anderson Cancer Center. A.S. was supported by the Summer Program in Cancer Research funded by the National Institutes of Health R25 CA181004.

CRediT authorship contribution statement **Angela H. Ting:** Writing – review & editing, Writing – original draft, Visualization, Supervision, Project administration, Funding acquisition, Conceptualization. **Byron H. Lee:** Writing – original draft, Investigation, Conceptualization. **Vishal Nanavaty:** Writing – review & editing, Investigation, Conceptualization. **Rosie Ou:** Writing – review & editing, Investigation. **Anwita Siddavatam:** Writing – review & editing, Investigation. **Briana Santo:** Writing – review & editing, Visualization, Methodology, Formal analysis. **Yi Zhang:** Writing – review & editing, Methodology, Investigation, Formal analysis. **Emily E. Fink:** Writing – original draft, Methodology, Investigation, Formal analysis, Conceptualization.

Data availability statement ChIP-seq data are available under accession number GEO:GSE131606. Hi-C-seq data are available under accession number PRJNA895385.

Declarations of interest The authors declare the following financial interests/personal relationships, which may be considered as potential competing interests. Angela H. Ting reports that financial support was provided by the National Institutes of Health and the National Cancer Institute. Emily E. Fink reports that financial support was provided by the National Institutes of Health and the National Cancer Institute. If there are other authors, they declare that they have no known competing financial interests or personal relationships that could have appeared to influence the work reported in this paper.

Acknowledgments We acknowledge the Proteomics and Metabolomics Core at the Lerner Research Institute, Cleveland Clinic, for their expert assistance in performing the mass spectrometry analyses in the DNA pulldown experiment.

Appendix A. Supplementary data

Supplementary data associated with this article can be found online at doi:10.1016/j.cstres.2025.100084.

References

1. Weindling E, Bar-Nun S. Sir2 links the unfolded protein response and the heat shock response in a stress response network. *Biochem Biophys Res Commun.* 2015;457:473–478.
2. Fink EE, Moparthy S, Bagati A, et al. XBP1-KLF9 axis acts as a molecular rheostat to control the transition from adaptive to cytotoxic unfolded protein response. *Cell Rep.* 2018;25:212–223.e214.
3. Richter K, Haslbeck M, Buchner J. The heat shock response: life on the verge of death. *Mol Cell.* 2010;40:253–266.
4. Chakrabarti A, Chen AW, Varner JD. A review of the mammalian unfolded protein response. *Biotechnol Bioeng.* 2011;108:2777–2793.
5. Zheng D, Wang R, Ding Q, et al. Cellular stress alters 3′UTR landscape through alternative polyadenylation and isoform-specific degradation. *Nat Commun.* 2018;9:2268.
6. Janssens S, Pulendran B, Lambrecht BN. Emerging functions of the unfolded protein response in immunity. *Nat Immunol.* 2014;15:910–919.
7. Sadek J, Omer A, Hall D, Ashour K, Gallouzi IE. Alternative polyadenylation and the stress response. *Wiley Interdiscip Rev RNA.* 2019;10:e1540.
8. Yoon OK, Brem RB. Noncanonical transcript forms in yeast and their regulation during environmental stress. *RNA.* 2010;16:1256–1267.
9. Liu X, Hoque M, Larochelle M, et al. Comparative analysis of alternative polyadenylation in *S. cerevisiae* and *S. pombe*. *Genome Res.* 2017;27:1685–1695.

10. Devany E, Park JY, Murphy MR, et al. Intronic cleavage and polyadenylation regulates gene expression during DNA damage response through U1 snRNA. *Cell Discov.* 2016;2:16013.
11. Fontana GA, Rigamonti A, Lenzken SC, et al. Oxidative stress controls the choice of alternative last exons via a Brahma-BRCA1-CstF pathway. *Nucleic Acids Res.* 2017;45:902–914.
12. Kreuz S, Fischle W. Oxidative stress signaling to chromatin in health and disease. *Epigenomics.* 2016;8:843–862.
13. Livernois AM, Mallard BA, Cartwright SL, Canovas A. Heat stress and immune response phenotype affect DNA methylation in blood mononuclear cells from Holstein dairy cows. *Sci Rep.* 2021;11:11371.
14. Vinoth A, Thirunalasundari T, Shanmugam M, Uthrakumar A, Suji S, Rajkumar U. Evaluation of DNA methylation and mRNA expression of heat shock proteins in thermal manipulated chicken. *Cell Stress Chaperones.* 2018;23:235–252.
15. Ramos-Lopez O, Riezu-Boj JI, Milagro FI, Martinez JA, Project M. DNA methylation signatures at endoplasmic reticulum stress genes are associated with adiposity and insulin resistance. *Mol Genet Metab.* 2018;123:50–58.
16. Kirchner H, Sinha I, Gao H, et al. Altered DNA methylation of glycolytic and lipogenic genes in liver from obese and type 2 diabetic patients. *Mol Metab.* 2016;5:171–183.
17. Han H, Hu J, Lau MY, Feng M, Petrovic LM, Ji C. Altered methylation and expression of ER-associated degradation factors in long-term alcohol and constitutive ER stress-induced murine hepatic tumors. *Front Genet.* 2013;4:224.
18. Palsamy P, Bidasee KR, Ayaki M, Augusteyn RC, Chan JY, Shinohara T. Methylglyoxal induces endoplasmic reticulum stress and DNA demethylation in the Keap1 promoter of human lens epithelial cells and age-related cataracts. *Free Radic Biol Med.* 2014;72:134–148.
19. Nanavaty V, Abrash EW, Hong C, et al. DNA methylation regulates alternative polyadenylation via CTCF and the cohesin complex. *Mol Cell.* 2020;78:752–764.e756.
20. Yabe I, Tanino M, Yaguchi H, et al. Pathology of frontotemporal dementia with limb girdle muscular dystrophy caused by a DNAJB6 mutation. *Clin Neurol Neurosurg.* 2014;127:10–12.
21. Couthouis J, Raphael AR, Siskind C, et al. Exome sequencing identifies a DNAJB6 mutation in a family with dominantly-inherited limb-girdle muscular dystrophy. *Neuromuscul Disord.* 2014;24:431–435.
22. Nam TS, Li W, Heo SH, et al. A novel mutation in DNAJB6, p.(Phe91Leu), in childhood-onset LGMD1D with a severe phenotype. *Neuromuscul Disord.* 2015;25:843–851.
23. Gillis J, Schipper-Krom S, Juenemann K, et al. The DNAJB6 and DNAJB8 protein chaperones prevent intracellular aggregation of polyglutamine peptides. *J Biol Chem.* 2013;288:17225–17237.
24. McMahon S, Bergink S, Kampinga HH, Ecroyd H. DNAJB chaperones suppress destabilised protein aggregation via a region distinct from that used to inhibit amyloidogenesis. *J Cell Sci.* 2021;134.
25. Rodriguez-Gonzalez C, Lin S, Arkan S, Hansen C. Co-chaperones DNAJA1 and DNAJB6 are critical for regulation of polyglutamine aggregation. *Sci Rep.* 2020;10:8130.
26. Kakkar V, Mansson C, de Mattos EP, et al. The S/T-Rich motif in the DNAJB6 chaperone delays polyglutamine aggregation and the onset of disease in a mouse model. *Mol Cell.* 2016;62:272–283.
27. Folke J, Arkan S, Martinsson I, et al. DNAJB6b is downregulated in synucleinopathies. *J Parkinsons Dis.* 2021;11:1791–1803.
28. Smith C, D'Mello SR. Cell and context-dependent effects of the heat shock protein DNAJB6 on neuronal survival. *Mol Neurobiol.* 2016;53:5628–5639.
29. Jiang B, Zhao Y, Shi M, et al. DNAJB6 promotes ferroptosis in esophageal squamous cell carcinoma. *Dig Dis Sci.* 2020;65:1999–2008.
30. Yu VZ, Wong VC, Dai W, et al. Nuclear localization of DNAJB6 is associated with survival of patients with esophageal cancer and reduces AKT signaling and proliferation of cancer cells. *Gastroenterology.* 2015;149:1825–1836.e1825.
31. Yuan X, Zhou Q, Zhang F, et al. Identification of immunity- and ferroptosis-related genes for predicting the prognosis of serous ovarian cancer. *Gene.* 2022;838:146701.
32. Zhang TT, Jiang YY, Shang L, et al. Overexpression of DNAJB6 promotes colorectal cancer cell invasion through an IQGAP1/ERK-dependent signaling pathway. *Mol Carcinog.* 2015;54:1205–1213.
33. Zhang Y, Yang Z, Cao Y, et al. The Hsp40 family chaperone protein DnaJB6 enhances Schlafen1 nuclear localization which is critical for promotion of cell-cycle arrest in T-cells. *Biochem J.* 2008;413:239–250.
34. Mitra A, Rostas JW, Dyess DL, Shevde LA, Samant RS. MicroRNA-632 downregulates DNAJB6 in breast cancer. *Lab Invest.* 2012;92:1310–1317.
35. Mitra A, Fillmore RA, Metge BJ, et al. Large isoform of MRJ (DNAJB6) reduces malignant activity of breast cancer. *Breast Cancer Res.* 2008;10:R22.
36. Deshayes N, Arkan S, Hansen C. The molecular chaperone DNAJB6, but not DNAJB1, suppresses the seeded aggregation of alpha-synuclein in cells. *Int J Mol Sci.* 2019;20.
37. Bason M, Meister-Broekema M, Alberts N, et al. Astrocytic expression of the chaperone DNAJB6 results in non-cell autonomous protection in Huntington's disease. *Neurobiol Dis.* 2019;124:108–117.
38. Hong YM, Hong Y, Choi YG, et al. The short isoform of DNAJB6 protects against 1-methyl-4-phenylpridinium ion-induced apoptosis in LN18 cells via inhibiting both ROS formation and mitochondrial membrane potential loss. *Oxid Med Cell Longev.* 2017;2017:7982389.
39. Sarparanta J, Jonson PH, Golzio C, et al. Mutations affecting the cytoplasmic functions of the co-chaperone DNAJB6 cause limb-girdle muscular dystrophy. *Nat Genet.* 2012;44:450–455.S451-452.
40. Mansson C, van Cruchten RTP, Weininger U, et al. Conserved S/T residues of the human chaperone DNAJB6 are required for effective inhibition of Abeta42 amyloid fibril formation. *Biochemistry.* 2018;57:4891–4902.
41. Xu X, Tao Y, Gao X, et al. A CRISPR-based approach for targeted DNA demethylation. *Cell Discov.* 2016;2:16009.
42. Ray J, Munn PR, Vihervaara A, et al. Chromatin conformation remains stable upon extensive transcriptional changes driven by heat shock. *Proc Natl Acad Sci USA.* 2019;116:19431–19439.
43. Weintraub AS, Li CH, Zamudio AV, et al. YY1 is a structural regulator of enhancer-promoter loops. *Cell.* 2017;171:1573–1588.e1528.
44. Schwalie PC, Ward MC, Cain CE, et al. Co-binding by YY1 identifies the transcriptionally active, highly conserved set of CTCF-bound regions in primate genomes. *Genome Biol.* 2013;14:R148.
45. Beagan JA, Duong MT, Titus KR, et al. YY1 and CTCF orchestrate a 3D chromatin looping switch during early neural lineage commitment. *Genome Res.* 2017;27:1139–1152.
46. Verheul TCJ, van Hijfte L, Perenthaler E, Barakat TS. The why of YY1: mechanisms of transcriptional regulation by Yin Yang 1. *Front Cell Dev Biol.* 2020;8:592164.
47. Alagar Boopathy LR, Jacob-Tomas S, Alecki C, Vera M. Mechanisms tailoring the expression of heat shock proteins to proteostasis challenges. *J Biol Chem.* 2022;298:101796.

48. Kmiecik SW, Mayer MP. Molecular mechanisms of heat shock factor 1 regulation. *Trends Biochem Sci.* 2022;47:218–234.
49. Hillary RF, FitzGerald U. A lifetime of stress: ATF6 in development and homeostasis. *J Biomed Sci.* 2018;25:48.
50. Yoshida H, Okada T, Haze K, et al. ATF6 activated by proteolysis binds in the presence of NF-Y (CBF) directly to the cis-acting element responsible for the mammalian unfolded protein response. *Mol Cell Biol.* 2000;20:6755–6767.
51. Masser AE, Kang W, Roy J, et al. Cytoplasmic protein misfolding titrates Hsp70 to activate nuclear Hsf1. *Elife.* 2019;8.
52. Zou J, Guo Y, Guettouche T, Smith DF, Voellmy R. Repression of heat shock transcription factor HSF1 activation by HSP90 (HSP90 complex) that forms a stress-sensitive complex with HSF1. *Cell.* 1998;94:471–480.
53. Hentze N, Le Breton L, Wiesner J, Kempf G, Mayer MP. Molecular mechanism of thermosensory function of human heat shock transcription factor Hsf1. *Elife.* 2016;5.
54. Ye J, Rawson RB, Komuro R, et al. ER stress induces cleavage of membrane-bound ATF6 by the same proteases that process SREBPs. *Mol Cell.* 2000;6:1355–1364.
55. Li M, Baumeister P, Roy B, et al. ATF6 as a transcription activator of the endoplasmic reticulum stress element: thapsigargin stress-induced changes and synergistic interactions with NF-Y and YY1. *Mol Cell Biol.* 2000;20:5096–5106.
56. Tahiliani M, Koh KP, Shen Y, et al. Conversion of 5-methylcytosine to 5-hydroxymethylcytosine in mammalian DNA by MLL partner TET1. *Science.* 2009;324:930–935.
57. He YF, Li BZ, Li Z, et al. Tet-mediated formation of 5-carboxylcytosine and its excision by TDG in mammalian DNA. *Science.* 2011;333:1303–1307.
58. Ito S, Shen L, Dai Q, et al. Tet proteins can convert 5-methylcytosine to 5-formylcytosine and 5-carboxylcytosine. *Science.* 2011;333:1300–1303.
59. Abayev-Avraham M, Salzberg Y, Gliksberg D, Oren-Suissa M, Rosenzweig R. DNAJB6 mutants display toxic gain of function through unregulated interaction with Hsp70 chaperones. *Nat Commun.* 2023;14:7066.
60. Kwon B, Fansler MM, Patel ND, Lee J, Ma W, Mayr C. Enhancers regulate 3′ end processing activity to control expression of alternative 3′UTR isoforms. *Nat Commun.* 2022;13:2709.
61. Westerheide SD, Anckar J, Stevens Jr SM, Sistonen L, Morimoto RI. Stress-inducible regulation of heat shock factor 1 by the deacetylase SIRT1. *Science.* 2009;323:1063–1066.
62. Rhee I, Bachman KE, Park BH, et al. DNMT1 and DNMT3b cooperate to silence genes in human cancer cells. *Nature.* 2002;416:552–556.
63. Wu KK. Analysis of protein-DNA binding by streptavidin-agarose pulldown. *Methods Mol Biol.* 2006;338:281–290.
64. Raudvere U, Kolberg L, Kuzmin I, et al. g:Profiler: a web server for functional enrichment analysis and conversions of gene lists (2019 update). *Nucleic Acids Res.* 2019;47:W191–W198.
65. Rohde C, Zhang Y, Reinhardt R, Jeltsch A. BISMA–fast and accurate bisulfite sequencing data analysis of individual clones from unique and repetitive sequences. *BMC Bioinformatics.* 2010;11:230.
66. Hagege H, Klous P, Braem C, et al. Quantitative analysis of chromosome conformation capture assays (3C-qPCR). *Nat Protoc.* 2007;2:1722–1733.
67. Lu L, Liu X, Huang WK, et al. Robust Hi-C maps of enhancer-promoter interactions reveal the function of non-coding genome in neural development and diseases. *Mol Cell.* 2020;79:521–534.e515.
68. Zhang SS, Plummer D, Lu LN, et al. DeepLoop robustly maps chromatin interactions from sparse allele-resolved or single-cell Hi-C data at kilobase resolution. *Nat Genet.* 2022;54:1013.
69. Kolde R, Kolde MR. Package 'pheatmap'. *R Package.* 2015;1:790.
70. Kassambara A, Mundt F. Package 'factoextra'. Extract and visualize the results of multivariate data analyses. 2017:76.
71. Heinz S, Benner C, Spann N, et al. Simple combinations of lineage-determining transcription factors prime cis-regulatory elements required for macrophage and B cell identities. *Mol Cell.* 2010;38:576–589.
72. Karolchik D, Baertsch R, Diekhans M, et al. The UCSC genome browser database. *Nucleic Acids Res.* 2003;31:51–54.